ASPS Conference Proceedings 1: 1621-1631 (2022)

Proceedings of

12th Structural Engineering Convention-An International Event (SEC 2022)

Available at https://asps-journals.com/index.php/acp

Performance of Supplemental Inertial Devices for Base-Isolated Structures

R. S. Jangid [1,*]

[1] Department of Civil Engineering, Indian Institute of Technology Bombay, Powai, Mumbai 400 076, India

Paper ID - 180464

Abstract

The seismic response of base-isolated structures with supplemental inertial devices subjected to stationary and real earthquake excitation is presented. Three types of devices, namely inertial mass damper (IMD), tuned mass damper-inerter (TMDI), and clutching inerter damper (CID), are considered. The seismic response of the base-isolated structure with and without inertial devices is compared to assess their effectiveness. Under stationary white-noise excitation, the optimum parameters of these devices were obtained. The criterion selected for optimality is the minimization of the mean-square relative displacement and absolute acceleration of the isolated structure. An equivalent linearization method was used for base-isolated structures with CID under stochastic excitation. It was observed that the IMD is not very effective in controlling the response of base-isolated structures. Optimally designed TMDI, on the other hand, was found to be effective in controlling the displacement and acceleration response of the isolated structure, with the effectiveness increasing as the inertance mass ratio increased. The CID involved in the base-isolated structure reduces the structural natural frequency and increases structural damping, thereby reducing isolator displacement and structural acceleration. The high-frequency components were present in the absolute acceleration of base-isolated structure with inertial devices (more pre-dominating for IMD and CID), which may have detrimental effects on installed high-frequency sensitive equipment.

Keywords: Clutching inerter damper, inertial mass damper, seismic base isolation, stationary excitation, structural acceleration, tuned mass damper-inerter

1. Introduction

During earthquakes, seismic base isolation is an effective way to protect structures and their contents. The principle of base isolation is to decouple the superstructure from its substructure resting on shaking ground, thus protecting its integrity. The introduction of base isolators between the superstructure and substructure decreases the system's fundamental frequency to a value lower than the predominant energy-containing frequencies of the earthquake, which enables the structure to survive a potentially devastating seismic force. The base isolation system can be used for both the new design of the structure and retrofitting. Several types of base isolation systems have been developed in the field of advanced seismic protection of structures during the past 40 years. Some of them are now widely used in practical applications, and especially in new design and retrofit of strategic buildings, such as hospitals, barracks, firehouses, emergency management headquarters, etc. [1,2].

Inerter-based dampers have recently gained tremendous popularity in the field of structural vibration control [3]. The inerter is a two-terminal inertial element with a large mass enhancement effect whose resisting force is proportional to the relative acceleration between two terminals [4,5]. The performance of inertial devices as a damper was also studied in buildings [6-8]. The improvement in buildings' performance was observed and demonstrated that the two parallel inerter devices with ratchet/clutching effects are more effective than a single inerter [7,8]. Later, some studies on clutching inerter damper (CID) were made for seismic response control of structures and found effective [9,11]. Recently, improvement in the performance of a base-isolated structure with supplemental inertial devices and tuned mass damper-inerter (TMDI) was also demonstrated [12-21]. The TMDI has been shown to be effective at controlling the response of base-isolated structures. Despite the above studies of inertial devices for base-isolated structures, there is further need to study their comparative performance and optimum parameters, which will be helpful in the effective aseismic design of the base-isolated structure. Here-in, the seismic response of the base-isolated structure with various combinations of supplemental inertial devices is investigated. The specific objectives of the study are summarized as to (i) present the response analysis of base-isolated structure with supplemental devices, namely IMD, TMDI, and CID under stationary earthquake excitation, (ii) obtain the optimum parameters for minimising the isolated structure's displacement and acceleration response, (iii) investigate their comparative performance in controlling the response under filtered white-noise excitation, and (iv) to study the effects of superstructure flexibility on the performance of IMD, TMDI and CID devices under real earthquake excitation.

2. Base-Isolated Structure with IMD

Figure 1 depicts a rigid mass structural model of a multi-story base-isolated structure connected with inerter / inertial mass

*Corresponding author. Tel: +912225767346; E-mail address: rsjangid@civil.iitb.ac.in

Published online: December 19, 2022

doi:10.38208/acp.v1.698

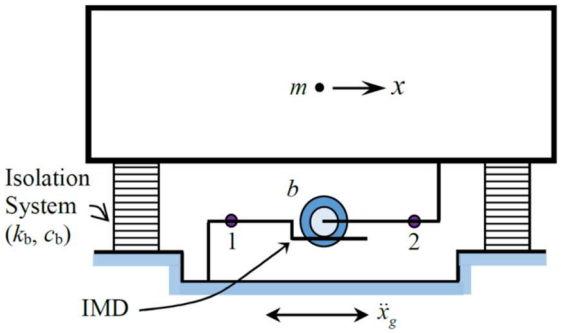

Fig. 1. Structural model of a base-isolated building with IMD.

damper (IMD) installed on stiff chevron frame support. The IMD employs a rack−pinion−flywheel system consisting of a flywheel with concentric to the flywheel, and there is an attached pinion engaged to a linear rack connected to the isolation floor. The IMD's movement generates a reaction force that is proportional to the relative acceleration between the two terminals, to a reasonable degree of accuracy. This proportional coefficient is the inertance or apparent mass, which can be several times the inerter's actual mass. Hence, the physical mass of the IMD is negligible when compared to its inertance. The mass, m is intended to represent the superstructure and the mass of the base floor above the isolation system. The isolation system designed for the building is considered as an equivalent linear force-deformation behaviour. The equivalent stiffness and damping of isolation are represented by k_b, c_b. The inertance of the IMD is denoted by b.

The isolation system and IMD considered can be characterized by the three parameters, namely, ω_b, ξ_b, and β defined as

$$\omega_b = \sqrt{\frac{k_b}{m}} \quad , \quad 2\xi_b\omega_b = \frac{c_b}{m}, \quad \text{and} \quad \beta = \frac{b}{m} \tag{1}$$

The governing equation of motion of base-isolated structure with IMD under earthquake excitation is expressed as

$$(m + b)\ddot{x} + c_b\dot{x} + k_b x = -m\ddot{x}_g \tag{2}$$

where x is the displacement of the isolated structure relative to ground; and $\ddot{x}_g$ is the earthquake ground acceleration. A dot over symbols signifies differentiation with respect to time t.

Dividing the equation (2) by $(m+b)$ and substituting $\beta = b/m$, the equation of motion reduces to

$$\ddot{x} + 2\left(\frac{\xi_b}{\sqrt{1+\beta}}\right)\left(\frac{\omega_b}{\sqrt{1+\beta}}\right)\dot{x} + \left(\frac{\omega_b}{\sqrt{1+\beta}}\right)^2 x = -\left(\frac{1}{1+\beta}\right)\ddot{x}_g \tag{3}$$

The above indicates that IMD elongates the vibration period and decreases the damping ratio of the base-isolated structure. It also suppresses the level of earthquake shaking (as the denominator on the right-hand side is always larger than unity).

The absolute acceleration of the base-isolated structural mass $\ddot{x}_a$ is expressed as

$$\ddot{x}_a = (\ddot{x} + \ddot{x}_g) = -(2\xi_b\omega_b\dot{x} + \omega_b^2 x + \beta\ddot{x}) \tag{4}$$

Interestingly, a term $\beta\ddot{x}$ is added in the absolute acceleration of the mass compared to the conventional isolation system, and it will be interesting to see its effects.

The entire base shear, V in the base-isolated structure will be

$$V = V_{is} + V_{in} \tag{5}$$

$$V_{is} = c_b\dot{x} + k_b x \quad \text{and} \quad V_{in} = b\ddot{x} \tag{6}$$

where V_{is} and V_{in} denote the shear in the isolation system and IMD, respectively.

Since the IMD has resistance to relative acceleration, the large force from the isolated structure may be transmitted to the supporting chevron brace. Because of this, it is evaluated and compared with the corresponding isolation force. The response quantities of interest in the present study are x, $\ddot{x}_a$, V_{is} and V_{in}.

2.1 *Frequency Response Function*

Assuming such a harmonic earthquake acceleration as $\ddot{x}_g = e^{j\omega t}$, where ω is the circular frequency and $j = \sqrt{-1}$, the steady-state responses are written as

$$x = H_x(j\omega)\, e^{j\omega t} \quad \text{and} \quad \ddot{x}_a = H_{\ddot{x}_a}(j\omega)\, e^{j\omega t} \tag{7a}$$

$$V_{is} = H_{V_{is}}(j\omega)\, e^{j\omega t} \quad \text{and} \quad V_{in} = H_{V_{in}}(j\omega)\, e^{j\omega t} \tag{7b}$$

where $H_x(j\omega)$, $H_{\ddot{x}_a}(j\omega)$, $H_{V_{is}}(j\omega)$ and $H_{V_{in}}(j\omega)$ are the frequency response function (FRF) of the responses x, $\ddot{x}_a$, V_{is} and V_{in}, respectively.

In Figure 2, the variation of FRF of various response quantities is plotted. Because of the added supplement inertial mass by the IMD, the resonating frequency for all responses decreases as the inertance-mass ratio increases.

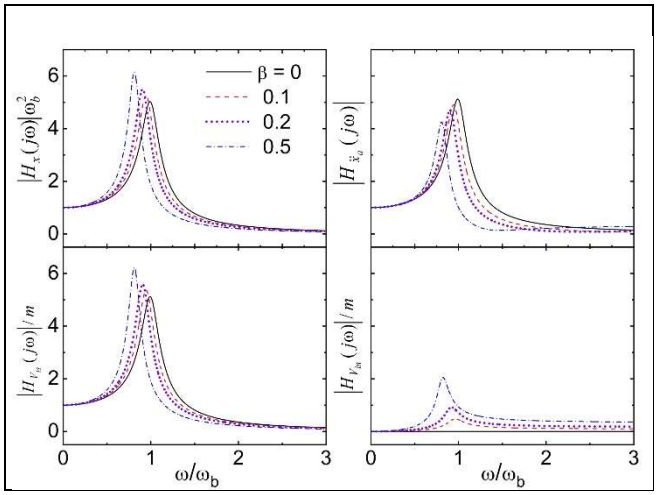

Fig. 2. FRF of base-isolated structure with IMD ($\omega_b = \pi$ rad/sec and ξ_b =0.1).

The resonating frequency for all the responses will be in the vicinity of $\omega_b/\sqrt{1+\beta}$ as per the structural dynamics [22]. The peak value of displacement response increases with the increase in the inertance-mass ratio. This is happening due to a decrease in the effective damping ratio (i.e. the damping ratio decrease to $\xi_b/\sqrt{1+\beta}$ and thereby increase the peak displacement response by $\sqrt{1+\beta}$ times). The peak values of absolute acceleration decrease with the increase of the β. However, for higher frequencies, the amplitude of absolute acceleration increases with the β implying that IMD will transmit earthquake vibrations into the base-isolated structures associated with the higher frequencies. This can be detrimental to the sensitive higher frequency equipment installed in the isolated structure. The variation of the FRF for the isolator force is quite similar to that observed for the isolator displacement. The isolator force at higher frequencies diminishes. However, the force in the IMD increases with the increase of the β and contains non-diminishing components at higher frequencies. Thus, it can be concluded that the IMD increases the peak displacement of the base-isolated structure. Further, due to the addition of the term $\beta\ddot{x}$ in the expression of the absolute acceleration of the base-isolated structure with IMD, its peak value is decreased but increased for the higher frequencies.

2.2 *Mean-Square Response under White-Noise Excitation*

The earthquake excitation is assumed to be a white-noise random process with zero mean. Let S_0 denote the constant power spectrum ordinate of the earthquake acceleration. The mean square responses of interest are expressed as

$$\sigma_x^2 = \int_{-\infty}^{\infty} \left|H_x(j\omega)\right|^2 S_0\, d\omega \tag{8a}$$

$$\sigma_{\ddot{x}_a}^2 = \int_{-\infty}^{\infty} \left|H_{\ddot{x}_a}(j\omega)\right|^2 S_0\, d\omega \tag{8b}$$

$$\sigma_{V_{is}}^2 = \int_{-\infty}^{\infty} \left|H_{V_{is}}(j\omega)\right|^2 S_0\, d\omega \tag{8c}$$

$$\sigma_{V_{in}}^2 = \int_{-\infty}^{\infty} \left|H_{V_{in}}(j\omega)\right|^2 S_0\, d\omega \tag{8d}$$

It is to be noted that the $\sigma_{\ddot{x}_a}^2 \to \infty$ and $\sigma_{V_{in}}^2 \to \infty$ when calculated from the above expressions. These responses become unbounded because of non-diminishing components in their FRF, as observed in Figure 2. This unbounded response is unrealistic, and to overcome this, the integration is to be carried out up to a cut-off (maximum) frequency, ω_c, above which the energy of the earthquake ground acceleration is considered negligible. The traditional value of this cut-off frequency is 33 Hz being used in the practicing design standards [23]. However, this frequency also appears to be conservative for the base-isolated structure having a natural frequency around 0.5 Hz and will unnecessarily increase the response. Thus, a more realistic value of the ω_c =100 rad/sec (roughly half of the 33 Hz) is used based on the filtered white-noise model of earthquake spectral density suggested by Clough and Penzien [24]. For the firm soil spectra [25], at this cut-off frequency, the spectrum ordinate is 0.0185 times the corresponding peak value. The root mean square (RMS) value of earthquake acceleration with the white-noise model is 1.46 times to the filtered white-noise model.

The mean-square responses obtained from equation (8) are further normalized by dividing the corresponding response of base-isolated structure without inertial device i.e.

$$\tilde{\sigma}_x^2 = \frac{\sigma_x^2}{\sigma_{x,0}^2},\ \tilde{\sigma}_{\ddot{x}_a}^2 = \frac{\sigma_{\ddot{x}_a}^2}{\sigma_{\ddot{x}_a,0}^2},\quad \tilde{\sigma}_{V_{is}}^2 = \frac{\sigma_{V_{is}}^2}{\sigma_{V_{is},0}^2} \text{ and } \tilde{\sigma}_{V_{in}}^2 = \frac{\sigma_{V_{in}}^2}{\sigma_{V_{is},0}^2} \tag{9}$$

$$\sigma_{x,0}^2 = \frac{\pi S_0}{2\xi_b\omega_b^3} \text{ and } \sigma_{\ddot{x}_a,0}^2 = \pi S_0\omega_b\left(\frac{1}{2\xi_b} + 2\xi_b\right) \tag{10a}$$

$$\sigma_{V_{is},0}^2 = \pi S_0\omega_b m^2\left(\frac{1}{2\xi_b} + 2\xi_b\right) \tag{10b}$$

Normalized response values less than unity indicate that the control system is effective at reducing response. The normalized variance for displacement and shear force in isolation can be expressed as[26]

$$\tilde{\sigma}_x^2 = 1 \text{ and } \tilde{\sigma}_{V_{is}}^2 = 1 - \left(\frac{\beta}{1+\beta}\right)\left(\frac{4\xi_b^2}{1+4\xi_b^2}\right) \tag{11}$$

Figure 3 shows the variation of the normalized mean-square responses against the inertance-mass ratio, β. The displacement response remains unchanged, and the isolator force decreases very marginally with the increase of β (refer equation (11)). It is also observed from the figure that as the β increases, the absolute acceleration first decreases, attaining a minimum value and then increases with the increase of β. This indicates that there exists a value of β for which the absolute acceleration of the isolated structure attains the minimum value. The optimum value occurs at the inertance mass ratio as β^{opt}=0.25 for the present case, and there is about a 20 percent reduction in the mean-square absolute acceleration. As expected, the force in the IMD increases with the increase of β. At large values of the β there is no advantage of using IMD in controlling the response, but there is a disadvantage of an increase of the entire base shear of base-isolated structure. In general, it can be concluded that the IMD is not very effective in controlling the response of the base-isolated structure.

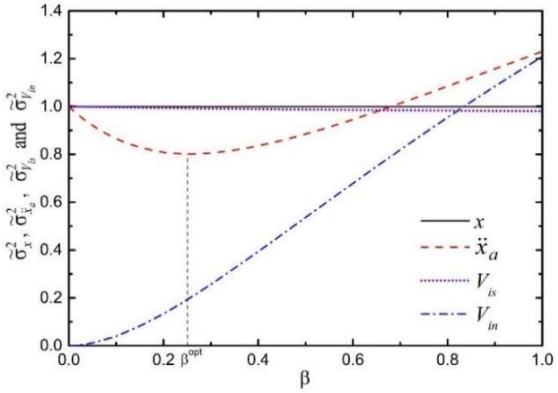

Fig. 3. Normalized mean-square responses of base-isolated structure with IMD (ω_b = π rad/sec and ξ_b =0.1).

3. Base-Isolated Structure with TMDI

The schematic diagram of the TMDI installed in the base-isolated structure is shown in Figure 4. This device consists of an auxiliary mass (m_t), stiffness (k_t), and damper (c_t) referred as TMD and an inertial device with inertance as b. The inertial device is connected to vibrating auxiliary mass and the ground. The vibration of the isolated structure causes resonance in the TMD and it dissipates the energy through damping. The performance of the TMD device increases with the increase of the TMD mass, m_t. Since it is not possible to physically provide a large mass, the attached inertial device can enhance the value without increasing the overall physical mass. The TMDI system considered can be characterized by the four parameters defined as

$$\alpha_m = \frac{m_t}{m}, \quad \alpha_c = \frac{c_t}{c_b}, \quad \alpha_k = \frac{k_t}{k_b} \text{ and } \beta = \frac{b}{m} \tag{12}$$

The two nodes, marked as 1 and 2 in figure 4 are connected to the corresponding nodes in the model of Figure 1 of the base-isolated structure. The governing equations of motion are

$$\begin{bmatrix} m & 0 \\ 0 & m_t + b \end{bmatrix} \begin{Bmatrix} \ddot{x} \\ \ddot{x}_t \end{Bmatrix} + \begin{bmatrix} c_b + c_t & -c_t \\ -c_t & c_t \end{bmatrix} \begin{Bmatrix} \dot{x} \\ \dot{x}_t \end{Bmatrix} + \begin{bmatrix} k_b + k_t & -k_t \\ -k_t & k_t \end{bmatrix} \begin{Bmatrix} x \\ x_t \end{Bmatrix} = -\begin{Bmatrix} m \\ m_t \end{Bmatrix} (\ddot{x}_g) \tag{13}$$

The FRF of the responses x, $\ddot{x}_a$, V_{is} and V_{in}, were obtained by solving the equation (13) in the frequency domain. The corresponding mean-square response under white-noise earthquake excitation is obtained by using the equation (8). In the case of the TMDI, the shear force in the inertial device will be $V_{in} = b\ddot{x}_t$.

The TMDI is most effective for lower values of α_m and higher values of β and therefore considered α_m=0.01 for all parametric variations [27]. The TMDI is most effective when the α_c and α_k are selected to the optimum values. To achieve this, an optimization problem is defined as

$$\text{minimize } \tilde{\sigma}_x^2 \quad \text{subject to} \quad \alpha_c \in \Omega_c, \ \alpha_k \in \Omega_k \tag{14a}$$

$$\text{minimize } \tilde{\sigma}_{\ddot{x}_a}^2 \quad \text{subject to} \quad \alpha_c \in \Omega_c, \ \alpha_k \in \Omega_k \tag{14b}$$

where Ω_k and Ω_c are the feasible regions for α_c and α_k, which are defined as positive orthants for the associated variables, respectively. The feasible regions considered are $0<\Omega_k<1$ and $0<\Omega_c<10$. An automated numerical search algorithm, α_c, and α_k spanning their ranges with increments of 10^{-4} to reach the desired accuracy are employed.

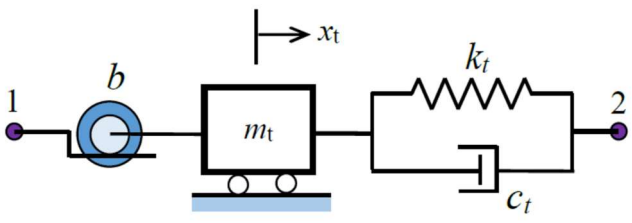

Fig. 4. Schematic diagram of TMDI.

A TMDI with optimum parameters for minimization of $\tilde{\sigma}_x^2$ and $\tilde{\sigma}_{\ddot{x}_a}^2$ is denoted as TMDI-D and TMDI-A, respectively. Table 1 shows the optimum parameters as well as the corresponding response for the TMDI-D. It can be noticed from this table that the optimum α_c^{opt} and α_k^{opt} increase by increasing β. The corresponding $\tilde{\sigma}_x^2$ and $\tilde{\sigma}_{\ddot{x}_a}^2$ decreases with the increase of β implying more effectiveness for higher inertance mass ratio. However, the reduction in the response because of TMDI-D for β>0.4 is marginal only. The V_{is} decreases, and V_{in} increases with the increasing β. However, there is a substantial reduction in the entire base shear of the isolated structure when TMDI-D is used and this phenomenon is opposite to that observed for the base-isolated structure with IMD. Table 2 shows the corresponding results of the TMDI-A. The main difference is that the optimal values of α_c and α_k obtained by minimizing the acceleration are generally greater than the corresponding ones obtained by minimizing the displacement.

An interesting trend of decrease of α_k^{opt} with an increase of β>0.8 is observed in Table 2. For large values of β, the TMDI-A acts like fixed support for the auxiliary stiffness (k_t) and damping (c_t) installed in the base-isolated structure. Under this condition, the base-isolated structure behaves like

Table 1. Optimal parameters and response of the TMDI-D for various values of β.

β	α_c^{opt}	α_k^{opt}	$\tilde{\sigma}_x^2$	$\tilde{\sigma}_{\ddot{x}_a}^2$	$\tilde{\sigma}_{V_{is}}^2$	$\tilde{\sigma}_{V_{in}}^2$
0	0.0047	0.0089	0.900	0.895	0.869	0
0.1	0.1578	0.0890	0.617	0.639	0.596	0.019
0.2	0.3780	0.1495	0.517	0.548	0.499	0.033
0.3	0.6200	0.1963	0.457	0.495	0.442	0.045
0.4	0.8697	0.2334	0.416	0.460	0.401	0.055
0.5	1.1203	0.2637	0.384	0.434	0.371	0.064
0.6	1.3649	0.2882	0.359	0.416	0.347	0.073
0.7	1.6054	0.3089	0.339	0.402	0.327	0.081
0.8	1.8394	0.3263	0.322	0.391	0.311	0.089
0.9	2.0672	0.3409	0.307	0.382	0.296	0.096
1	2.2864	0.3538	0.294	0.376	0.284	0.103

Table 2. Optimal parameters and response of the TMDI-A for various values of β.

β	α_c^{opt}	α_k^{opt}	$\tilde{\sigma}_x^2$	$\tilde{\sigma}_{\ddot{x}_a}^2$	$\tilde{\sigma}_{V_{is}}^2$	$\tilde{\sigma}_{V_{in}}^2$
0	0.0049	0.0098	0.907	0.889	0.876	0
0.1	0.2313	0.1156	0.658	0.600	0.636	0.020
0.2	0.6630	0.2141	0.580	0.492	0.560	0.039
0.3	1.2290	0.2997	0.534	0.429	0.515	0.058
0.4	1.8548	0.3685	0.499	0.389	0.481	0.078
0.5	2.4750	0.4186	0.467	0.363	0.451	0.098
0.6	3.0442	0.4528	0.439	0.347	0.424	0.116
0.7	3.5329	0.4680	0.411	0.337	0.396	0.132
0.8	3.9507	0.4697	0.385	0.332	0.371	0.145
0.9	4.2860	0.4541	0.36	0.329	0.348	0.154
1	4.5600	0.4257	0.338	0.329	0.327	0.160
∞	**4**	**0**	**0.2**	**0.385**	**0.2**	**0.123**

a single-degree-of-freedom system with total stiffness as k_b+k_t and damping as c_b+c_t. The mean square absolute acceleration for such system under white-noise earthquake excitation is expressed as [26]

$$\sigma^2_{\ddot{x}_a} = \frac{\pi S_0 \omega_b}{2\xi_b}\left(\frac{1+\alpha_k}{1+\alpha_c}\right) + 2\pi S_0 \omega_b \xi_b (1+\alpha_c) \qquad (15)$$

For the minimum value of the $\sigma^2_{\ddot{x}_a}$

$$\frac{\partial \sigma^2_{\ddot{x}_a}}{\partial \alpha_c} = 0 \text{ and } \frac{\partial \sigma^2_{\ddot{x}_a}}{\partial \alpha_k} = 0 \qquad (16)$$

By carrying out the above partial differentiation and simplifying

$$\alpha_c^{opt} = \frac{1}{2\xi_b} - 1 \text{ and } \alpha_k^{opt} = 0 \qquad (17)$$

For ξ_b=0.1, the corresponding $\alpha_c^{opt} = 4$. The optimum parameters and corresponding response when $\beta \to \infty$ are shown in Table 2. At $\alpha_c^{opt} = 4$, the overall damping ratio of the base-isolated structure is 0.5, which is equal to the classical optimum damping for the linear and nonlinear base-isolated structures [28,29].

The variation of FRF of various response quantities of base-isolated structure with TMDI-D and TMDI-A is plotted in Figure 5. The inertance-mass ratio is considered as 0.2, and the FRF responses are compared with the corresponding base-isolated structure without TMDI (referred to as BIS). The FRF of isolated structure with TMDI appears to be a two-peaked response, and the optimization of parameters takes place when the response to the second peak is minimized for both cases of TMDI-D and TMDI-A. The other interesting phenomenon observed in the figure is that the high-frequency amplitudes are not present in the absolute acceleration response of the base-isolated structure. However, the high-frequency amplitudes are present in the FRF of $V_{in,}$ but their amplitude is relatively small compared to the corresponding FRF of V_{in} of the base-isolated structure with IMD.

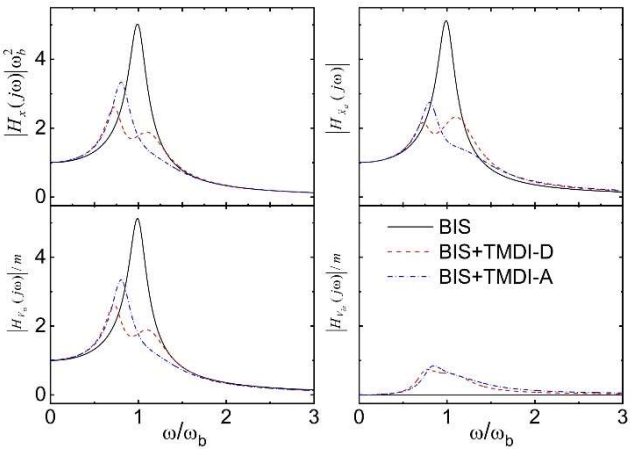

Fig. 5. FRF of base-isolated structure with TMDI-D and TMDI-A (ω_b = π rad/sec and ξ_b =0.1).

4. Base Isolated Structure with CID

A simple IMD was found to be ineffective in controlling the response of a base-isolated structure earlier in the present study. Furthermore, after the structure reaches its peak velocity and begins to slow down, the IMD or its support may be subjected to a significant force. To counteract these effects, the CID is considered, which is redesigned with two flywheels on both sides and a chevron brace to support it, as shown in Figure 6. Both flywheels have a ratchet between the gear and the flywheel, but the direction of the ratchet is opposite for both flywheels. The ratchet in the CID has a clutching effect that allows the flywheel to break away from the structure, preventing the flywheel from pushing the structure. In contrast to the IMD, this device can accelerate the decay of velocity and reduce the displacement response in this way [10].

The restoring force of the CID with inertance as b is expressed as

$$V_{in} = \begin{cases} b\ddot{x} & \text{when } (\dot{x}\,\ddot{x}) > 0 \\ 0 & \text{when } (\dot{x}\,\ddot{x}) \le 0 \end{cases} \qquad (18)$$

The above equation indicates that the CID posses with inherent non-linearity. The nonlinear behavior of the CID can be replaced with the equivalent linearized model by

$$V_{in} = b_{eq}\ddot{x} + c_{eq}\dot{x} \qquad (19)$$

where b_{eq} and c_{eq} are equivalent inertance and the equivalent damping of the CID, respectively.

The two nodes, marked as 1 and 2 in figure 6, are connected to the corresponding nodes in the model of base-isolated shown Figure 1. The equation of motion of the base-isolated structure with CID can be expressed as

$$(m + b_{eq})\ddot{x} + (c_b + c_{eq})\dot{x} + k_b x = -m\ddot{x}_g \qquad (20)$$

The above equation reveals that there will be a reduction in structural frequency and added damping for a base-isolated structure with CID. These effects usually help control the seismic response of structures.

The values of b_{eq} and c_{eq} can be obtained by minimizing the expectation of the difference between linear and nonlinear terms [26]. Using this technique, the values of the b_{eq} and c_{eq} were obtained by Li and Liang [10] and are given by

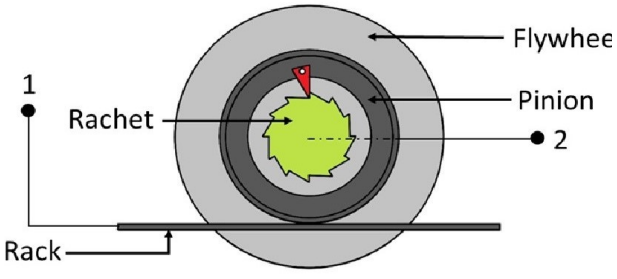

Fig. 6. Schematic diagram of CID.

$$b_{eq} = (1+\beta-\sqrt{1+\beta})m \qquad (21)$$

$$c_{eq} = \frac{\beta m}{\pi}\frac{\sigma_{\ddot{x}}}{\sigma_{\dot{x}}} \qquad (22)$$

where $\sigma_{\ddot{x}}$ and $\sigma_{\dot{x}}$ denote the RMS relative acceleration and velocity of the base-isolated structure, respectively.

The FRF of the responses x, $\ddot{x}_a$, V_{is} and V_{in}, are obtained by solving the equation (20) in the frequency domain. The corresponding mean-square responses under white-noise earthquake excitation with S_0=0.05 m^2/sec^3 are obtained by using the equation (8). To avoid the unbounded response, the cut-off frequency is selected as 100 rad/sec, which is the same used earlier for the IMD.

In Figure 7, the variation of FRF of various responses is plotted. It can be observed that the resonance frequency is reduced as the inertance-mass ratio grows, which demonstrates the influence of the CID on structural frequency reduction. There is also a reduction of the peak resonance response due to the added damping property of the CID. At higher frequencies, the amplitude of absolute acceleration increases with the increased β implying that the CID will transmit the vibration into base-isolated structures associated with higher frequencies. The isolator force at higher frequencies diminishes; however, the force in the CID increases with the increase of β and contains non-diminishing components. To summarize, the CID involved in the isolated structure will reduce the structural natural frequency and increase structural damping, thereby reducing both relative isolator displacement and absolute structural acceleration.

Figure 8 shows the variation of the normalized mean square responses of the base-isolated structure with CID. The displacement goes on decreasing with the increase of the inertance-mass ratio. The figure also observes that with an increase in the inertance-mass ratio, the structural acceleration reduces first and attains a minimum value, and then it increases with the increase of the inertance-mass ratio. This indicates that there exists an optimum inertance-mass

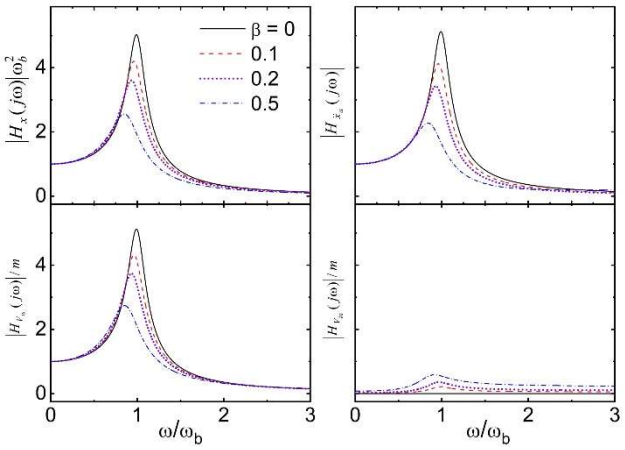

Fig. 7. FRF of base-isolated structure with CID ($\omega_b = \pi$ rad/sec and ξ_b =0.1).

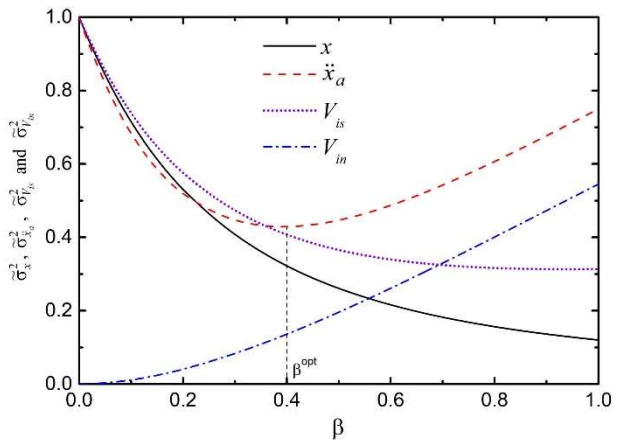

Fig. 8. Normalized mean-square responses of base-isolated structure with CID ($\omega_b = \pi$ rad/sec and ξ_b =0.1).

ratio of the CID for which the absolute structural acceleration attains the minimum value. The optimum value occurs for β^{opt}=0.4, and there is a 58 percent reduction in the mean-square absolute acceleration. This behavior of the CID is quite similar to that observed for the frictional elements in the sliding isolation systems and viscous damping and yield strength in elastomeric bearings [28-31]. As expected, the force in the isolation system decreases, and force in the CID increases with the increase of β. At larger values of the β, the force in the CID is higher than that of isolation system isolation. In general, it can be concluded that the CID is quite effective in controlling the response of the base-isolated structure, and there exists an optimum inertance-mass ratio of the CID for which the absolute structural acceleration attains the minimum value.

5. Response to Filtered White Noise Excitation

The power spectral density function (PSDF) of the earthquake acceleration, $\ddot{x}_g$ is considered as that suggested by Clough and Penzien [24] i.e.

$$S_{\ddot{x}_g}(\omega) = S_0\left(\frac{1+4\xi_g^2(\omega/\omega_g)^2}{[1-(\omega/\omega_g)^2]^2+4\xi_g^2(\omega/\omega_g)^2}\right)\times \left(\frac{(\omega/\omega_f)^4}{[1-(\omega/\omega_f)^2]^2+4\xi_f^2(\omega/\omega_f)^2}\right) \qquad (23)$$

where S_0 is the constant PSDF of input white-noise random process; ω_g and ξ_g are the predominant frequency and damping ratio of the primary (soil media) filter, and ω_f and ξ_f are the secondary filter parameters. For the present study, the values selected are S_0=0.05 m^2/sec^3, ω_g=15 rad/sec, ξ_g=0.6, ω_f=1.5 rad/sec and ξ_f=0.6 which correspond to a site with firm soil profile [25].

A comparison of the optimum values of the stiffness and damping for the TMDI system for the base-isolated structure is shown in Figure 9. It is seen that the optimized parameters are not much altered for lower values of inertance-mass ratio (i.e., β<0.4) under the filtered white-noise model for the minimization of both responses. However, the difference in the optimum parameters increases with the increasing of β and ~~it~~ is more pronounced for the parameters of minimization

of acceleration ~~in~~ compared to the corresponding for minimization of displacement.

In Figure 10, the normalized mean square responses under filtered white-noise earthquake acceleration are plotted against the β for base-isolated structure with IMD, TMDI-D, TMDI-A and CID. The response normalization is performed using the corresponding response without an inertial device under the same earthquake excitation. The pattern of the response of the isolated structure is similar to that observed earlier for the white-noise excitation. The optimum value of the β for the minimum absolute acceleration response for IMD and CID was observed to be increased in comparison with the white-noise excitation. The IMD is most effective when β is around 0.4; after that, the acceleration response remains more or less constant. The performance of the CID is also observed to be comparable with that of the TMDI-D and TMDI-A for β>0.4. However, for the same inertance ratio, there is more cost involved in the case of TMDI due to the installation of additional auxiliary mass, stiffness, and damping devices (refer to Tables 1 and 2 for required values which are pretty substantial).

6. Response to Real Earthquake Excitation

The rigid base-isolated structure's response with TMDI and CID showed that these devices are very good at controlling the response under stationary unfiltered and filtered white-noise excitation. However, it will be interesting to investigate

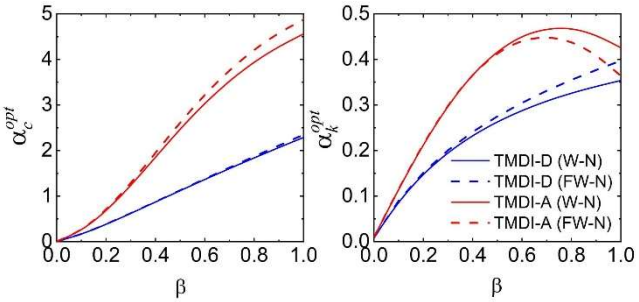

Fig. 9. Comparison of optimum parameters of the TMDI-D and TMDI-A under white-noise (W-N) and filtered white-noise (FW-N) excitation (ω_b = π rad/sec and ξ_b =0.1).

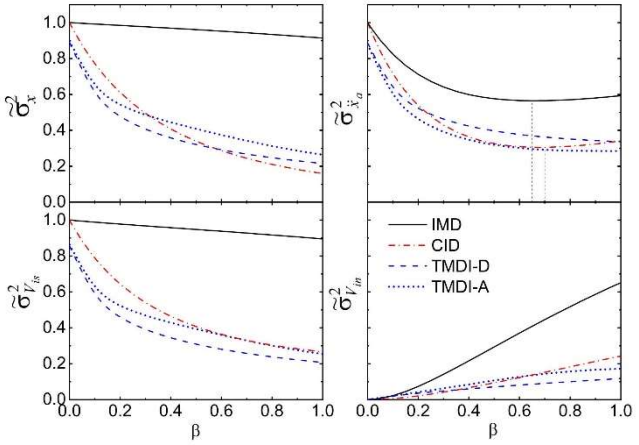

Fig. 10. Normalized mean-square responses of base-isolated structure with IMD, TMDI-D, TMDI-A, and CID under filtered white-noise excitation (ω_b = π rad/sec and ξ_b =0.1).

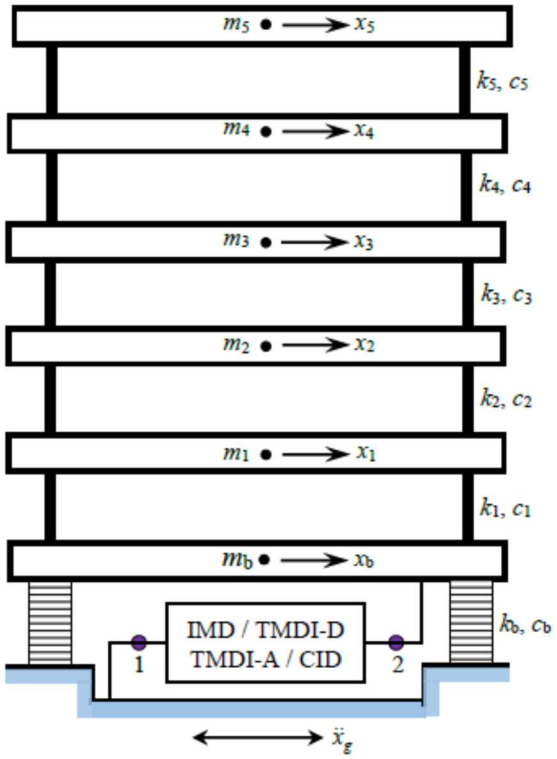

Fig. 11. Structural model of a flexible base-isolated building with IMD, TMDI-D, TMDI-A, and CID.

their effectiveness under actual earthquake excitation and by considering base-isolated structure as flexible, which will provide insight into the frequency contents of the superstructure accelerations and the tuning behavior of the TMDI. Figure 11 shows a model of a flexible base-isolated building installed with inertial devices such as IMD, TMDI, and CID. For this building with inertial devices at the isolator level, the governing equations of motion is

$$\mathbf{M}\,\ddot{\mathbf{x}}(t)+\mathbf{C}\,\dot{\mathbf{x}}(t)+\mathbf{K}\,\mathbf{x}(t)+\mathbf{D}\,\mathbf{F}_s(t)=-\mathbf{E}\,\ddot{x}_g(t) \qquad (24)$$

where **M**, **C**, and **K** = mass, damping, and stiffness matrices of the base-isolated building, respectively; **x**(*t*) represents the horizontal displacements (relative to the ground) vector of each mass at time *t*; **D** is the location matrix for the vector of control forces $\mathbf{F}_s(t)$ produced by the inertial devices; **E** is the vector containing the vibrating masses; and $\ddot{x}_g(t)$ is the earthquake acceleration. The seismic response of the isolated building with inertial devices is evaluated by numerically integrating the equations of motion [22].

A five-story building with base isolation is selected for the present study, and its parameters are taken from Kelly [32]. The parameters are: $m_1 = m_2 = m_3 = m_4 = m_5 = m_b$ (i.e. same mass at all floors and base raft locations). The inter-story stiffness of different floors is taken as $k_1 = 15k$, $k_2 = 14k$, $k_3 = 12k$, $k_4 = 9k$ and $k_5 = 5k$. The value of k is selected to provide the fundamental period of the fixed base-superstructure as 0.4 sec. The five natural frequencies of the superstructure with a fixed base measured in rad/sec are 15.71, 38.48, 60.84, 83.12, and 105.37. The damping matrix of the superstructure is constructed by assuming the modal damping ratio of 0.02 in all modes of vibration. The isolation

system is designed such that the isolation frequency is π rad/sec and the isolation damping ratio is 0.1. The inertance-mass ratio β=0.4 is considered for all the IMD, TMDI-D, TMDI-A, and CID. The corresponding auxiliary mass, damping, and stiffness values for TMDI-D and TMDI-A are taken from Tables 1 and 2, respectively. Two recorded earthquake motions, namely the N90E component of the 1994 Northridge earthquake (recorded at Sylmar Station) and the N00E component of the 1995 Kobe earthquake (recorded at JMA) with 30 secs durations, are selected. Northridge and Kobe earthquake motions' peak ground acceleration (PGA) are 0.6*g* and 0.83*g*, respectively. The response quantities of interest are the relative base displacement (x_b), base shear forces, and top floor absolute acceleration ($\ddot{x}_5^a$). The base shear forces are normalized with the total weight of isolated building *W*.

The time variation of relative base displacement of isolated structure with IMD, TMDI-D, TMDI-A, and CID is shown in Figure 12 and compared with the corresponding displacement of the isolated structure without inertial devices (referred to as BIS). The figure reveals that the TMDI-D, TMDI-A, and CID effectively reduce the base displacement under both earthquakes. The reduction in the base displacement is in the range of 30 to 40 percent. The base displacement of isolated structures with IMD was observed to be the same for the Northridge earthquake and decreased for the Kobe earthquake. This behavior is corresponding to the spectral displacement variation of these earthquakes. It was also observed from the figure that the base displacement is primarily associated with the fundamental frequency of the isolated structure. Thus, the TMDI-D, TMDI-A, and CID add damping in a base-isolated structure and effectively limit the base displacements.

Figures 13 and 14 show the time variation of the top floor absolute acceleration of base-isolated structure with different inertial devices and earthquakes. The figure indicates that the peak top floor acceleration increased for IMD and CID compared to the corresponding base-isolated structure without inertial devices. This is expected as these devices are directly connected between ground and base mass/raft and therefore transmit the earthquake vibration into the superstructure. This phenomenon was observed in the FRF of absolute accelerations of the isolated structure with IMD and CID (refer to Figures 2 and 7). On the other hand, the top floor's absolute acceleration reduction for the base-isolated structure with TMDI-D, TMDI-A is observed. This figure also reveals that the high-frequency components are present in the absolute acceleration of base-isolated structure with inertial devices (more pre-dominating for IMD and CID) and may have detrimental effects on high-frequency sensitive types of equipment.

Figures 12 to 14 show that the peak response of base-isolated structures with TMDI occurs in the vicinity of the corresponding time for the peak response without TMDI. Further, there are not many cycles of the structure's response with TMDI that take place before the occurrence of the peak response. This indicates that the TMDI may not control the response of the base-isolated structure through tuning effects but controls it due to heavy damping (i.e., auxiliary damping c_t) of the TMDI [33].

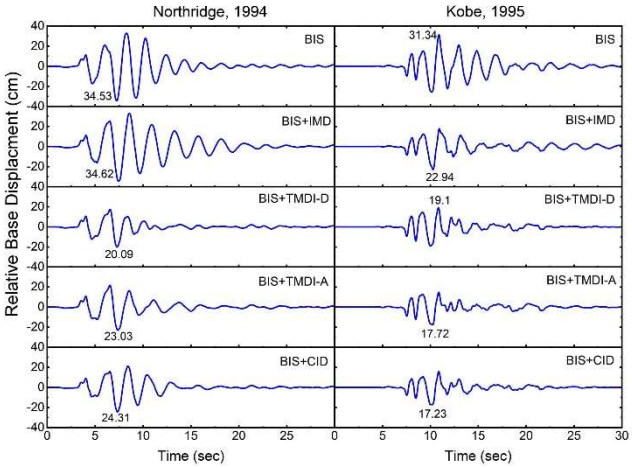

Fig. 12. Time variation of relative base displacement of isolated building with IMD, TMDI-D, TMDI-A and CID.

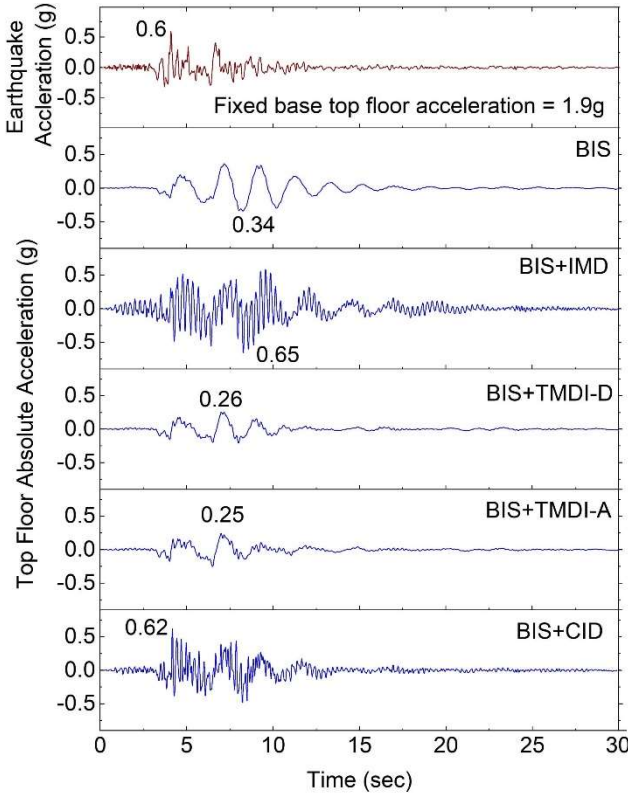

Fig. 13. Time variation of earthquake acceleration and top floor absolute acceleration of base-isolated building with IMD, TMDI-D, TMDI-A, and CID under Northridge, 1994 excitation.

To provide additional insight into the frequency characteristics of absolute accelerations of base-isolated structure with inertial devices, the fast Fourier transform (FFT) amplitude spectrum is computed and is presented in Figures 15 and 16. The red dashed vertical lines in these plots indicate the natural frequencies of the corresponding structure. The FFT of the acceleration of base-isolated structure has a dominating peak at isolation frequency with a small peak at the second natural frequency. The FFT of the acceleration of base-isolated structure with IMD and CID has a dominating peak at isolation frequency and second and third structural natural frequencies. On the other hand, the peak of

the FFT amplitude of acceleration of the isolated structure with TMDI-D and TMDI-A occurs in the vicinity of the first two natural frequencies of the isolated structure. For these devices, there are also contributions from the higher frequencies (up to nearly 3rd natural frequency) and more pronounced for TMDI-A as it has higher damping. The presence of high-frequency amplitudes in the accelerations of base-isolated structures with CID may also be attributed due to sudden change in stiffness (or mass) due to the nonlinear behavior of CID and the high-frequency modes getting excited during the nonlinear phase of the motion as a result of energy transfer from the adequately excited fundamental mode [34].

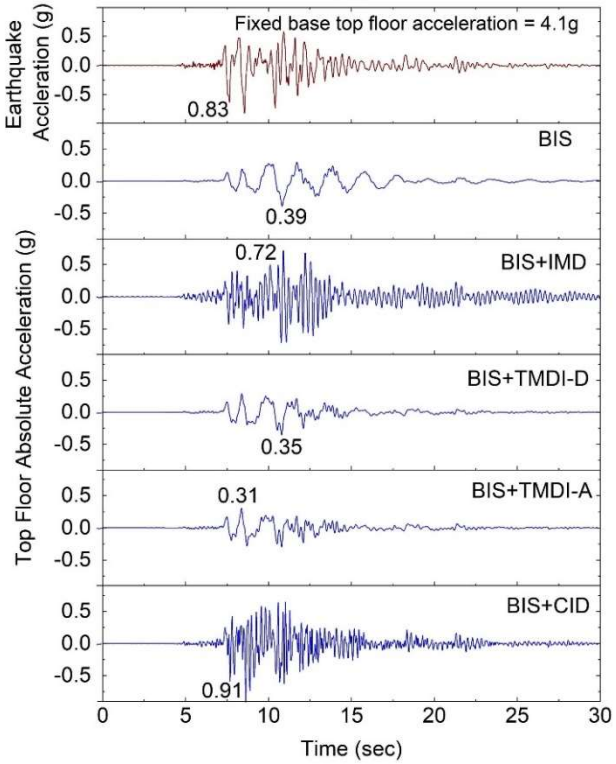

Fig. 14. Time variation of earthquake acceleration and top floor absolute acceleration of base-isolated building with IMD, TMDI-D, TMDI-A and CID under Kobe, 1995 excitation.

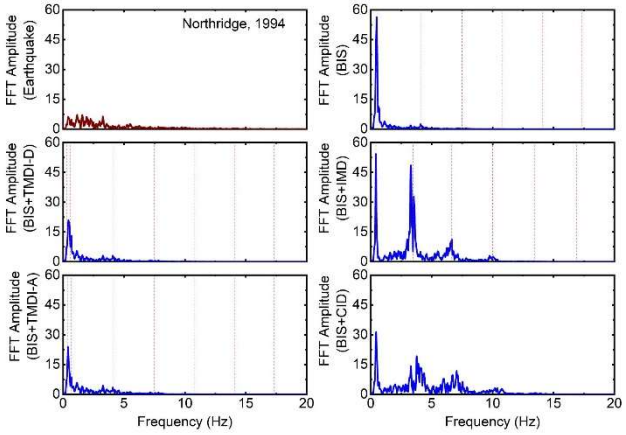

Figure 15. FFT Plots of earthquake acceleration and top floor absolute acceleration of base-isolated building with IMD, TMDI-D, TMDI-A, and CID under Northridge, 1994 excitation (red dashed vertical lines indicate natural frequencies).

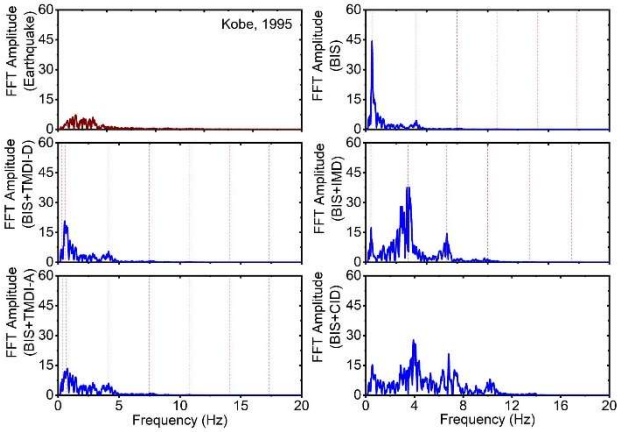

Fig. 16. FFT Plots of earthquake acceleration and top floor absolute acceleration of base-isolated building with IMD, TMDI-D, TMDI-A, and CID under Kobe, 1995 excitation (red dashed vertical lines indicate natural frequencies).

Table 3 shows the peak values of the corresponding normalized isolator, inerter, and total base shear forces. As expected, the shear force in the IMD is quite significant, confirming its ineffectiveness in controlling the response of the base-isolated structure. The shear force in CID is also relatively high, but it can reduce the shear force in the isolation system. The shear force in TMDI is minimum among all devices, and it is also reducing the isolator shear force. Thus, it can be concluded that the base shear in the TMDI is relatively less in comparison with the corresponding shear in the IMD and CID. Further, for all inertial devices, the peak value of the total base shear has not increased substantially from the corresponding peak of either isolator or inerter force. This is happening because the peak shear force in the isolator and inerter does not occur simultaneously and are more or less orthogonal to each other. The total base shear is also not exceeding the corresponding base shear for the BIS condition.

Table 3. Normalized shear force in inertial devices of the five-story base-isolated building.

Force (W)	Isolated Condition	Northridge, 1994	Kobe, 1995
Total or isolator shear force	BIS	0.35	0.31
Isolator shear force	BIS+IMD	0.36	0.23
	BIS+TMDI-D	0.21	0.20
	BIS+TMDI-A	0.24	0.18
	BIS+CID	0.25	0.18
Inerter shear force	BIS+IMD	0.22	0.34
	BIS+TMDI-D	0.10	0.11
	BIS+TMDI-A	0.12	0.15
	BIS+CID	0.19	0.27
Total shear force	BIS+IMD	0.31	0.28
	BIS+TMDI-D	0.25	0.26
	BIS+TMDI-A	0.21	0.22
	BIS+CID	0.25	0.29

7. Conclusions

The seismic response of base-isolated structures with supplemental inertial devices, namely IMD, TMDI, and CID, is investigated. The earthquake excitation is modeled as stationary stochastic as well as recorded time histories. The effectiveness of inertial devices is studied by comparing the response of the isolated structure with and without inertial devices. From the trends of the results of the present study, the following conclusions may be drawn:

1. The IMD increases the peak displacement of the base-isolated structure. Although the absolute peak acceleration is reduced, the IMD transmits vibrations to the base-isolated structure at higher frequencies.
2. The base-isolated structure's normalized mean-square displacement response with IMD remains unchanged, and the isolator force decreases only slightly as the inertance-mass ratio increases. The absolute acceleration decreases until it reaches a minimum value, then increases as the inertance-mass ratio rises. The force in the IMD increases as the inertance-mass ratio of the IMD rises. In general, the IMD does not appear to be very effective at controlling the response of the base-isolated structure.
3. Optimally designed TMDI-D and TMDI-A are found to be effective in controlling the displacement and acceleration response of the base-isolated structure, with their effectiveness increasing as the inertance-mass ratio increases. However, for inertance-mass ratios greater than 0.4, the response was only marginally reduced. The optimal values of TMDI parameters obtained by minimizing the acceleration are generally higher than those obtained by minimizing the displacement.
4. The CID involved in the isolated structure reduces the structural natural frequency and increases structural damping, thereby reducing both relative isolator displacement and absolute structural acceleration. In general, it can be concluded that the CID is quite effective in controlling the response of the isolated structure, and there exists an optimum inertance-mass ratio of the CID for which the absolute structural acceleration attains the minimum value.
5. The optimum values of the stiffness and damping of the TMDI under filtered white-noise earthquake excitation are not much altered for lower values of an inertance-mass ratio less than 0.4 compared with the corresponding values under white-noise excitation. However, the difference in the optimum parameters increases with the increase of inertance-mass ratio and is more pronounced for minimization of acceleration compared to the minimization of displacement.
6. The pattern of the response of the isolated structure with inertial devices under filtered white-noise earthquake excitation is observed to be similar to white-noise excitation. The performance of the CID is comparable with that of the TMDI for an inertance-mass ratio greater than 0.4. However, for the same inertance ratio, there is more cost involved in the case of TMDI for the installation of additional auxiliary mass, stiffness, and damping devices.
7. The TMDI in a base-isolated structure effectively limits the floor accelerations and base shear under actual earthquake excitation. The TMDI (especially with a large inertance-mass ratio) may not control the response of the base-isolated structure through tuning effects but controls it due to the heavy damping of its auxiliary damper.
8. The high-frequency components are observed to be present in the absolute acceleration of base-isolated structure with inertial devices (more pre-dominating for IMD and CID) and may have detrimental effects on installed high-frequency sensitive types of equipment.

Disclosures

Free Access to this article is sponsored by SARL ALPHA CRISTO INDUSTRIAL.

References

1. Naiem F, Kelly JM. Design of Seismic Isolated Structures: From Theory to Practice. John Wiley and Sons, NY, 1999.
2. Matsagar VA, Jangid RS. Base isolation for seismic retrofitting of structures. Practice Periodical on Structural Design and Construction, ASCE, 2008; 13(4):175-185.
3. Ma R, Bi K, Hao H. Inerter-based structural vibration control: A state-of-the-art review. Engineering Structures, 2021; 243: 112655.
4. Smith MC. Synthesis of mechanical networks: The inerter. IEEE Transactions on Automatic Control, 2002; 47(10): 1648-1662.
5. Chen MZQ, Papageorgiou C, Scheibe F, Wang F-C, Smith MC. The missing mechanical circuit element. IEEE Circuits and Systems Magazine, 2009; 9(1): 10-26.
6. Hwang J-S, Kim J, Kim Y-M. Rotational inertia dampers with toggle bracing for vibration control of a building structure. Engineering Structures, 2007; 29(6): 1201-1208.
7. Makris N, Kampas G. Seismic protection of structures with supplemental rotational inertia. Journal of Engineering Mechanics, ASCE, 2016; 142(11): 04016089.
8. Makris N, Moghimi G. Displacements and forces in structures with inerters when subjected to earthquakes. Journal of Structural Engineering, ASCE, 2019; 145(2): 04018260.
9. Wang M, Sun F. Displacement reduction effect and simplified evaluation method for SDOF systems using a clutching inerter damper. Earthquake Engineering and Structural Dynamics, 2018; 47(7): 1651-1672.
10. Li L, Liang Q. Seismic assessment and optimal design for structures with clutching inerter dampers. Journal of Engineering Mechanics, ASCE, 2020; 146(4): 04020016.
11. Jangid RS. Seismic performance assessment of clutching inerter damper for isolated bridges. Practice Periodical on Structural Design and Construction, ASCE, 2022; 27(2): 04021078.
12. Pradono MH, Iemura H, Igarashi A, Kalantari A. Application of angular-mass dampers to base-isolated benchmark building. Structural Control and Health Monitoring, 2008; 15(5): 737-745.

13. Saitoh M. On the performance of gyro-mass devices for displacement mitigation in base isolation systems. Structural Control and Health Monitoring, 2012; 19(2):246-259.

14. De Domenico D, Ricciardi G. An enhanced base isolation system equipped with optimal tuned mass damper inerter (TMDI). Earthquake Engineering and Structural Dynamics, 2018; 47(5): 1169-1192.

15. De Domenico D, Ricciardi G. Improving the dynamic performance of base-isolated structures via tuned mass damper and inerter devices: A comparative study. Structural Control and Health Monitoring, 2018; 25(10): e2234.

16. DeAngelis M, Giaralis A, Petrini F, Pietrosanti D. Optimal tuning and assessment of inertial dampers with grounded inerter for vibration control of seismically excited base-isolated systems. Engineering Structures, 2019; 196: 109250.

17. Li C, Chang K, Cao L, Huang Y. Performance of a nonlinear hybrid base isolation system under the ground motions. Soil Dynamics and Earthquake Engineering, 2021; 143: 106589.

18. Zhao Z, Zhang R, Jiang Y, Pan C. Seismic response mitigation of structures with a friction pendulum inerter system. Engineering Structures, 2019; 193:110-120.

19. De Domenico D, Ricciardi G, Zhang R. Optimal design and seismic performance of tuned fluid inerter applied to structures with friction pendulum isolators. Soil Dynamics and Earthquake Engineering, 2020; 132: 106099.

20. Jangid RS. Optimum tuned inerter damper for base-isolated structures. Journal of Vibration Engineering & Technologies, 2021; 9 (7): 1483-1497.

21. Jangid RS. Optimum parameters and performance of tuned mass damper-inerter for base-isolated structures. Smart Structures and Systems, 2022; 29(4): 549-560.

22. Chopra AK. Dynamics of Structures: Theory and Applications to Earthquake Engineering. 5th Edn, Pearson, 2017.

23. Regulatory Guide 1.60. Design response spectra for seismic design of nuclear power plants. U.S. Nuclear Regulatory Commission, 2014.

24. Clough RW, Penzien J. Dynamics of Structures. 3rd Edn, Berkeley, CA: Computers and Structures, 2003.

25. Kiureghian AD, Neuenhofer A. Response spectrum method for multi-support seismic excitations. Earthquake Engineering and Structural Dynamics, 1992; 21(8): 713-740.

26. Roberts JB, Spanos PD. Random vibration and statistical linearization. Chichester, Wiley UK, 1990.

27. Pietrosanti D, De Angelis M, Basili M. Optimal design and performance evaluation of systems with tuned mass damper inerter (TMDI). Earthquake Engineering and Structural Dynamics, 2017; 46(8): 1367-1388.

28. Inaudi JA, Kelly JM. Optimum damping in linear isolation systems. Earthquake Engineering and Structural Dynamics, 1993; 22(7): 583-598.

29. Jangid RS. Optimum damping in a nonlinear base isolation system. Journal of Sound and Vibration, 1996; 189(4): 477-487.

30. Jangid RS. Optimum frictional elements in sliding isolation system. Computers and Structures, 2000; 76(4): 651-661.

31. Jangid RS. Stochastic response of building frames isolated by lead-rubber bearings. Structural Control and Health Monitoring, 2010; 17(1): 1-22.

32. Kelly JM. Earthquake-resistant design with rubber, 2nd Edn, London: Springer-Verlag, 1997.

33. Villaverde R. Reduction in seismic response with heavily-damped vibration absorbers. Earthquake Engineering and Structural Dynamics, 1985; 13: 33-42.

34. Chakraborty S, Ray-Chaudhuri S. Energy transfer to high-frequency modes of a building due to sudden change in stiffness at its base. Journal of Engineering Mechanics, ASCE, 2017; 143(8): 04017050.